Processing and Application of Ceramics 10 [4] (2016) 257–264
DOI: 10.2298/PAC1604257B

Spark plasma sintering of hydrothermally synthesized bismuth ferrite

Zorica Branković[1,*], Danijela Luković Golić[1], Aleksandar Radojković[1], Jovana Ćirković[1], Damir Pajić[2], Zorica Marinković Stanojević[1], Junwei Xing[3], Miladin Radović[4], Guorong Li[5], Goran Branković[1]

[1]*Institute for Multidisciplinary Research, University of Belgrade, Kneza Višeslava 1a, 11030 Belgrade, Serbia*
[2]*Department of Physics, Faculty of Science, University of Zagreb, Bijenička cesta 32, HR-10000 Zagreb, Croatia*
[3]*Department of Mechanical Engineering, Texas A&M University, College Station, TX 77840, USA*
[4]*Department of Materials Science and Engineering Program, Texas A&M University, College Station, TX 77840, USA*
[5]*The State Key Lab of High Performance Ceramics and Superfine Microstructure, Shanghai Institute of Ceramics, Chinese Academy of Sciences, Shanghai 200050, People's Republic of China*

Received 19 August 2016; Received in revised form 17 November 2016; Accepted 2 December 2016

Abstract

Bismuth ferrite, $BiFeO_3$ (BFO), powder was synthesized by hydrothermal method from $Bi(NO_3)_3 \cdot 5\,H_2O$ and $Fe(NO_3)_3 \cdot 9\,H_2O$ as precursors. The synthesized powder was further sintered using spark plasma sintering (SPS). The sintering conditions were optimized in order to achieve high density, minimal amount of secondary phases and improved ferroelectric and magnetic properties. The optimal structure and properties were achieved after spark plasma sintering at 630 °C for 20 min, under uniaxial pressure of 90 MPa. The composition, microstructure, ferroelectric and magnetic properties of the SPS samples were characterized and compared to those of conventionally sintered ceramics obtained from the same powder. Although the samples sintered using conventional method showed slightly lower amount of secondary phases, the spark plasma sintered samples exhibited favourable microstructure and better ferroelectric properties.

Keywords: *perovskites, spark plasma sintering, microstructure, X-ray diffraction, magnetic properties*

I. Introduction

The most attractive feature of bismuth ferrite, $BiFeO_3$ (BFO), is a coexistence of ferroelectric and antiferromagnetic properties in a single phase at room temperature. Bismuth ferrite has a rhombohedral distorted perovskite structure (space group *R3c*) with lattice parameters a = 5.5775(5) Å, c = 13.8616(8) Å, α = 90°, γ = 120° [1]. It shows spontaneous polarization along one of the eight pseudo-cubic [111] axes below Curie temperature (T_C) of 826–845 °C, and antiferromagnetism below Néel temperature (T_N) of 370 °C [2,3]. Bismuth ferrite has several important properties, such as high remnant polarization (100 μC/cm^2 in a single crystal) and piezoelectricity, which makes it worth thorough investigation [4].

Nevertheless, there are several issues related to the synthesis and processing of polycrystalline bismuth ferrite. The most important are: thermodynamic instability of $BiFeO_3$ in the 447–767 °C temperature range, sensitivity to even very small amounts of impurities, and evaporation of Bi_2O_3 at higher temperatures, all of which lead to formation of the substantial amount of secondary phases in the final product, and difficult fabrication of high purity bulk samples [4,5]. Although various syntheses methods have been used to prepare $BiFeO_3$ powders, starting from solid state reaction to wet chemical methods (sol-gel, co-precipitation, hydrothermal, microwave-hydrothermal, sonochemical and auto-combustion methods) [6], formation of the secondary phases cannot be avoided in any of those methods, while their amount can be significantly lowered by careful optimization of the processing conditions. Several research teams have reported successful

* Corresponding author: tel: +381 11 208 5043,
fax: +381 11 2085038, e-mail: *zorica.brankovic@imsi.bg.ac.rs*

preparation of phase pure bismuth ferrite powders, using methods such as molten alkali metal salts [7] and mechanochemical synthesis [8–10]. Another important problem in fabrication of BFO ceramics is difficult densification of the powders during sintering. According to literature data, it is extremely difficult to reach densities exceeding 90 %TD (theoretical density) [5]. Some alternative sintering techniques, such as rapid liquid phase sintering [6–11] or microwave sintering of BFO [12], have been applied to improve both purity and density of the final product. Among different sintering methods, spark plasma sintering (SPS) has been recognized as a potentially efficient method of preparation of high-density and single phase BFO ceramics with improved dielectric, ferroelectric and magnetic properties [13]. For example, SPS of powders, previously treated in a high-energy ball mill, resulted in high-density BFO samples (density up to 97 %TD) [14,15]. Although several studies reported on SPS of BFO ceramics, the full potential of employing this sintering method in processing a fully dense, phase pure $BiFeO_3$ ceramics is not still sufficiently explored. For example, very limited data on magnetic properties of BFO ceramics, processed by SPS, were presented in some of those studies, indicating enhanced magnetization [16] of the SPS samples in comparison with the samples processed using more conventional sintering methods.

Most recently, we used hydrothermal method to synthesize a high purity $BiFeO_3$ powders (99.9% phase purity) with only 0.1 wt.% of $Bi_2Fe_4O_9$ as a secondary phase. Those high purity powders were further sintered in the bulk samples with 96 %TD after sintering [17] using combination of pressing at high pressure of 9 t/cm^2 (883 MPa) and conventional sintering at 800 °C for 2 h. Since the relative densities of the bulk BFO samples in that study are very close to the densities reached by SPS, we can conclude that these two methods are probably the most promising for preparation of high density bulk BFO ceramics.

In this paper, we compared composition, microstructure, ferroelectric and magnetic properties of bismuth ferrite ceramics sintered by spark plasma sintering and conventional methods. In both cases we used the same hydrothermally synthesized precursor powder. The ceramics samples were characterized by the same methods, under the same conditions. It was found that the samples prepared by SPS showed better ferroelectric and magnetic properties.

II. Material and methods

The chemical reagents used to prepare $BiFeO_3$ powder in this study were bismuth(III) nitrate pentahydrate ($Bi(NO_3)_3{\cdot}5\,H_2O$, Merck), iron(III) nitrate nonahydrate ($Fe(NO_3)_3{\cdot}9\,H_2O$, Merck), and potassium hydroxide (KOH, pelleted, Sigma Aldrich).

$BiFeO_3$ powder was synthesized by hydrothermal method from the $Bi(NO_3)_3{\cdot}5\,H_2O$ and $Fe(NO_3)_3{\cdot}9\,H_2O$ precursors. Detailed explanation of synthesis method is given in our previous article [17]. Two series of ceramic samples were prepared: samples sintered in conventional furnace (CFS samples) and spark plasma sintered (SPS samples).

CFS samples processing: Optimal processing conditions were chosen based on the previous study [17]. The powders were pressed under pressure of 9 t/cm^2 (883 MPa) into pellets of 6 mm in diameter and sintered at 800 °C, for 2 hours under ambient conditions in a tube furnace (heating rate of 5 °C/min).

SPS samples processing: Sintering was performed in the SPS (Model # SPS 25-10, Thermal Technology LLC) using a graphite die with the diameter of 16 mm. The samples were heated at different temperatures (600 to 700 °C) with heating rate of 100 °C/min, and held at the target temperature for 10 to 20 minutes under the constant flow of the ultra-high purity argon (99.999%). Uniaxial pressure of 90 MPa was applied before the heating cycle and maintained until the sample cooled to the ambient temperature with a cooling rate of 100 °C/min. Those sintering temperatures have been chosen based on the results of the previous studies [15,18,19]. All SPS samples are further denoted in this study as SPS(sintering temperature in °C)-(sintering time in min). Therefore, the sample SPS600-10 for example, denotes the sample sintered at 600 °C for 10 min. After sintering, the samples were annealed at 600 °C for 6 h, in air atmosphere to compensate for eventual oxygen non-stoichiometry after sintering in inert atmosphere.

The $BiFeO_3$ powder was examined by X-ray diffraction analysis (XRD) (D8 X-ray, Bruker). Unit cell parameters and phase composition were calculated using LSUCRI [20] and FullProf programs [21], respectively. Density of the samples was determined by Archimedes method, using alcohol immersion procedure described in more details elsewhere [22]. The microstructure of the powders and sintered samples was investigated by scanning electron microscopy (TESCAN Vega TS 5130 MM). The sintered samples were polished and further thermally etched at 720 °C for 45 minutes in the ambient air before SEM analysis.

Standard bipolar polarization hysteresis measurements of the samples were performed on Precision Multiferroic Test System (Radiant Technologies, Inc.). Precision Multiferroic Test System consists of Multiferroic Test Unit, High Voltage Interface Unit to 4000 V, and High Voltage Ampifier to 4000 V. Silver electrodes were applied on the samples before measurements, while the sample holder was made of platinum, providing good electrical contacts.

Magnetization hysteresis measurements were carried out using commercial MPMS5 SQUID magnetometer. Besides the usual temperature interval of 2–400 K, the oven inserted within this instrument was used to measure the magnetization in high temperature region of 300–800 K. Combining both temperature intervals the

real zero-field-cooled (ZFC) and field-cooled (FC) temperature dependences of magnetization were measured in constant applied field, together with magnetic hysteresis loops in magnetic fields up to 50 kOe (5 T) at several temperatures.

III. Results and discussion

According to XRD analysis (Fig. 1a), the starting powder was almost pure $BiFeO_3$ since it contained only 0.1 wt.% of the secondary $Bi_2Fe_4O_9$ phase [17]. XRD patterns of ceramics sintered by conventional method are compared to those of the SPS samples prepared at different sintering conditions (Figs. 1b-h).

The unit cell parameters of the CFS samples and as-sintered SPS samples (Table 1) were slightly larger than those provided in the literature for the rhombohedral bismuth ferrite (space group *R3c*) [1]. In addition, in the case of the SPS samples the parameter *a* slightly increased with sintering temperature. It can be seen from Table 1, that post sintering annealing at 600 °C had no influence on unit cell parameters, i.e., they can be consider identical to the parameters of the as-sintered samples taking into account accuracy of the fitting. The CFS sample contained less than 5 wt.% of typical secondary phases, $Bi_2Fe_4O_9$ and $Bi_{25}FeO_{39}$, as it was determined by Rietveld analysis of the XRD results (Table 2). Despite of the fact that many authors reported pure $BiFeO_3$ phase in ceramics obtained by SPS at temperatures between 625 and 650 °C [15,18,19], XRD results (Fig. 1) clearly indicate the presence of the secondary phases in all sintered samples, regardless of the sintering conditions. Comparison of XRD diffraction patterns of the SPS samples revealed that the lowest amount of the secondary phases was detected in the sample sintered at 600 °C. Their amount was found to increase with increase in sintering temperature and/or time of sintering. Post-sintering annealing resulted in decreased amount of the secondary phases, but could not completely eliminate them. The SPS600-10 contained only 3 wt.% of $Bi_2Fe_4O_9$ while $Bi_{25}FeO_{39}$ was not found in that sample after annealing. Secondary phases were present in both SPS630-20 and SPS650-10 samples (Table 2). The SPS630-20 sample contained approximately 8 wt.% of secondary phases, and amount of secondary phases sharply increased up to 15 wt.% in SPS650-10. Formation of the secondary phases in the SPS samples is related to partial loss of bismuth and oxygen during sintering in inert atmosphere [23], but we should also take into account carbon contamination that was found in some of our samples (Fig. 1g) and possibility that partial reduction occurred due to the contact between the samples and a graphite die. The graphite die can react with oxygen from the sample at temperatures above 600 °C that would further decrease oxygen partial pressure, especially in the pressing tool. CO is most likely the product of the reaction and its formation lead to the further reducing atmosphere and intensive gas phase transport between the sample and die. Reduction of oxides or even precipitation of carbides and carbon in the sample can occur as a final result of these processes [24]. Obviously, all these processes become more intensive with increase of temperature, and the non-stoichiometry is more pronounced and, probably, irreversible at some point. In the samples sintered above 650 °C, decomposition of BFO as well as reaction with carbon significantly increased, and those samples were dismissed for further investigation. The latter confirms the results of previous studies [23] showing that in some cases, a pure BFO cannot be obtained by SPS even after post-sintered annealing. Additionally, it has been shown that change of post-sintering annealing atmosphere can significantly affect the phase composition of BFO ceramics sintered by the SPS method. Wang *et al.* reported a pure BFO phase after annealing in oxygen atmosphere [23]. Although they found lower conductivity in oxygen-annealed samples than in ones annealed in air, some other authors came to the opposite conclusions [19]; they found increased conductivity in oxygen-annealed samples, and the reasons for this discrepancy are not clear at this moment. As a result of trade-off between single-phased ceramics and its conductivity, we choose air atmosphere as a compromise

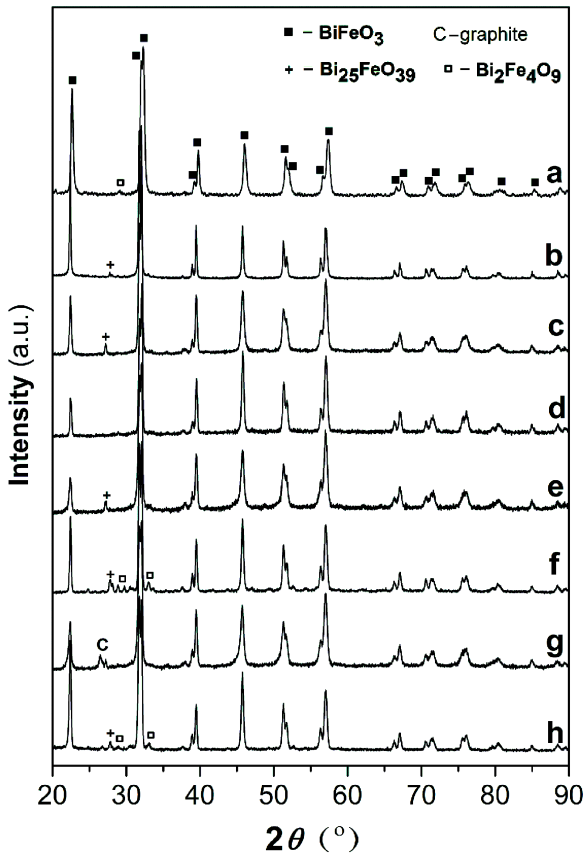

Figure 1. XRD patterns of: a) the starting BFO powder, b) CFS sample, c) as-sintered SPS600-10 sample, d) SPS600-10 sample after annealing, e) as-sintered sample SPS630-20, f) sample SPS630-20 after annealing, g) as-sintered sample SPS650-10, h) SPS650 -10 sample after annealing

Table 1. Unit cell parameters of some SPS samples before and after annealing in comparison to CFS sample and literature data

Sample	ICSD 157424[24]	CFS	SPS600-10 (as-sint.)	SPS600-10 (annealed)	SPS630-20 (as-sint.)	SPS630-20 (annealed)	SPS650-10 (as-sint.)	SPS 650-10 (annealed)
a (Å)	5.57414(4)	5.5776(2)	5.579(2)	5.576(1)	5.580(1)	5.580(1)	5.588(3)	5.582(1)
c (Å)	13.8588(1)	13.8618(6)	13.862(5)	13.861(4)	13.870(4)	13.871(5)	13.865(9)	13.868(6)

Table 2. The phase composition of CFS and SPS samples after annealing

Sample	CFS	SPS600-10	SPS630-20	SPS650-10
$BiFeO_3$ [wt.%]	95.8	97.0	92.3	84.8
$Bi_2Fe_4O_9$ [wt.%]	2.7	3.0	4.8	10.2
$Bi_{25}FeO_{39}$ [wt.%]	1.5	0.0	2.9	5.0

between these two requests. We can conclude that control of phase composition during spark plasma sintering of oxide ceramics is very delicate and demands careful and detailed optimization of sintering and post-sintering annealing conditions.

Microstructural analysis of the starting hydrothermally synthesized BFO powder showed mostly irregularly shaped submicron particles, with very few of them exceeding size of 1 μm, (Fig. 2a). SEM images in backscatter electrons (BSE) mode of the CFS sample in Fig. 2b reveals microstructure consisting of irregularly shaped grains. Most of the small grains have size below 1.5 μm, while the size of the larger ones ranged between 3 μm and 5 μm. The small content of $Bi_{25}FeO_{39}$ and $Bi_2Fe_4O_9$ phases was clearly observed in Fig. 2b as white and dark grey grains, respectively. The CFS samples, processed under optimal pressing and sintering conditions, reached 96 %TD [17], and we could not achieve such high densities by SPS. Serious deterioration of phase composition was observed at higher temperatures that were needed for better densification. Density of the SPS samples sintered at 600 °C was very low, about 74 %TD.

SEM analysis of the sample SPS600-10 also confirmed high porosity and incomplete sintering process (Fig. 2c). The grains are also irregularly shaped, significantly smaller than in the CFS sample, mostly ranging between 1 and 2 μm in size. Small amount of secondary phase was found in some parts of the sample. Increase of sintering temperature to 650 °C led to much higher densities, reaching 90 %TD. The grains of BFO in the sample SPS650-10 (Fig. 2d) have similar size and mor-

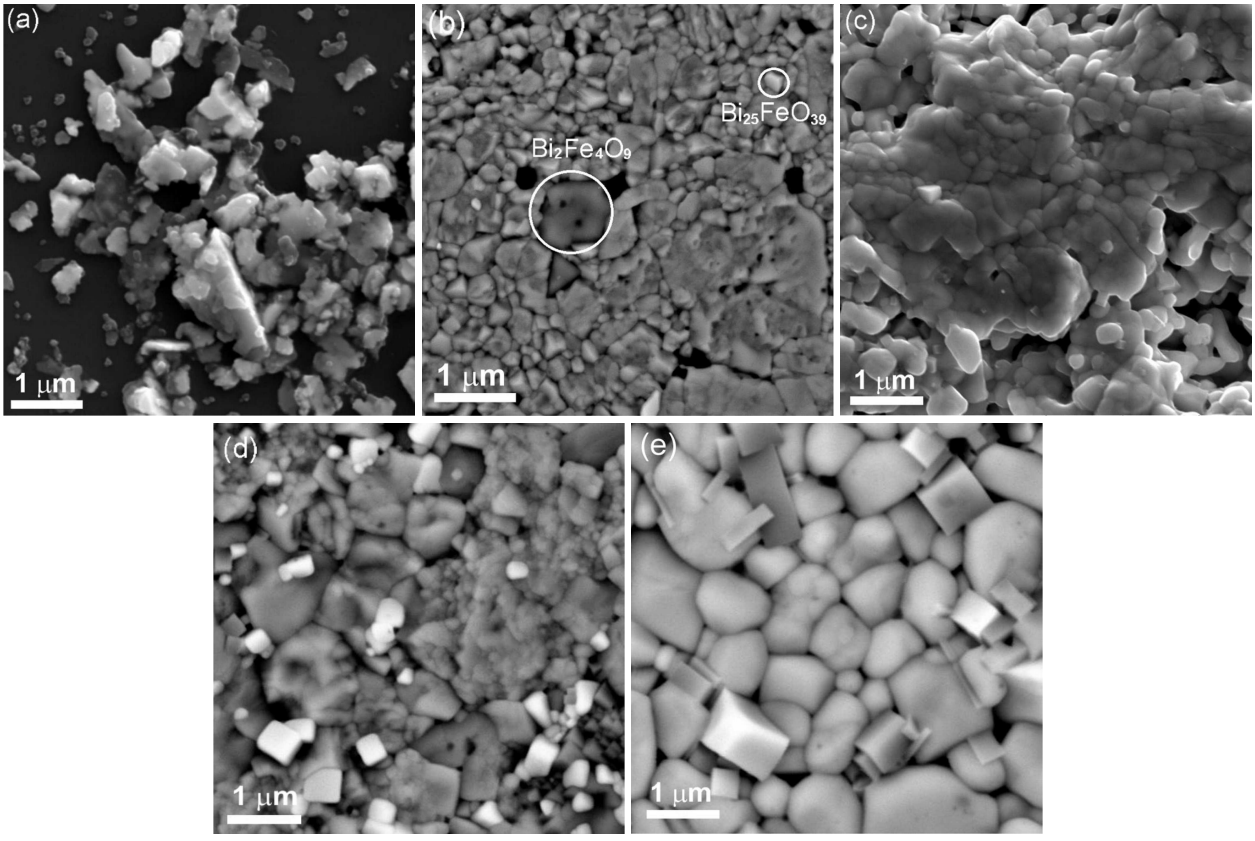

Figure 2. SEM micrographs of: a) the starting BFO powder, b) CFS sample, c) SPS600-10, d) SPS650-10, e) SPS630-20. All SPS samples were annealed

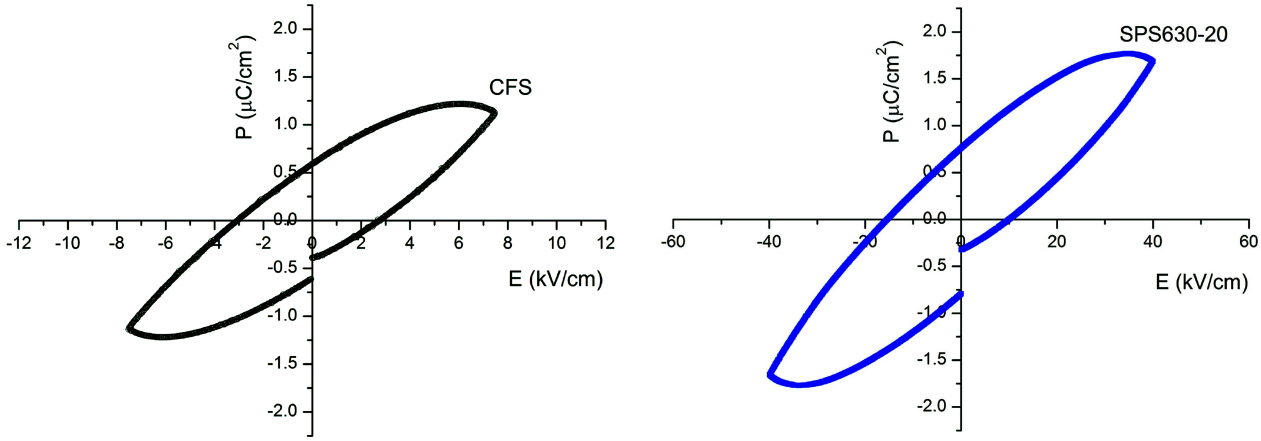

(a) (b)

Figure 3. Room temperature *P-E* hysteresis loops of samples: a) CFS and b) SPS630-20

phology as the grains in the CFS sample, but the amount of the secondary phases is higher. Decrease in sintering temperature to 630 °C and extension of sintering time to 20 min resulted in BFO ceramics (Fig. 2e) with similar density as in the sample SPS650-10, but with lower amount of the secondary phases. The sample SPS630-20 shows favourable microstructure in terms of better crystallinity, well defined grain boundaries and the absence of agglomerates.

Ferroelectric measurements were performed only for sufficiently dense samples, i.e. in those having relative densities above 90 %TD. The polarization (P) versus electric field (E) hysteresis loops of CFS and SPS630-20 samples are presented in Fig. 3. The values of remnant polarization (P_r) for both samples are relatively small, 0.59 μC/cm^2 and 0.76 μC/cm^2 for the CFS and SPS630-20, respectively, and they are in accordance with literature data [12,16,26–28]. The SPS630-20 sample exhibited significantly higher coercive field of 10.4 kV/cm compared with 2.77 kV/cm for the CFS sample. Also, the CFS sample could not withstand application of higher electric fields (>10 kV/cm). Significantly higher values of the breakdown fields in the SPS samples indicate lower leakage currents. The higher coercive field could be attributed to its larger grains, because a switching of ferroelectric domains is more difficult inside a large grain than in small one [29]. A less roundish shape of the hysteresis loop confirms that a leakage current is lower in the SPS sample (Fig. 3), which is interesting as it contains slightly higher amount of the secondary phases. Even more importantly, the SPS samples can also contain higher concentration of oxygen vacancies that contributes to low resistance of the sample due to the reduction atmosphere during sintering, as mentioned in discussion of XRD results. Obviously, some other features, such as Fe^{2+} ions concentration should be considered, since electron hopping between Fe^{2+} and Fe^{3+} can increase leakage current, too

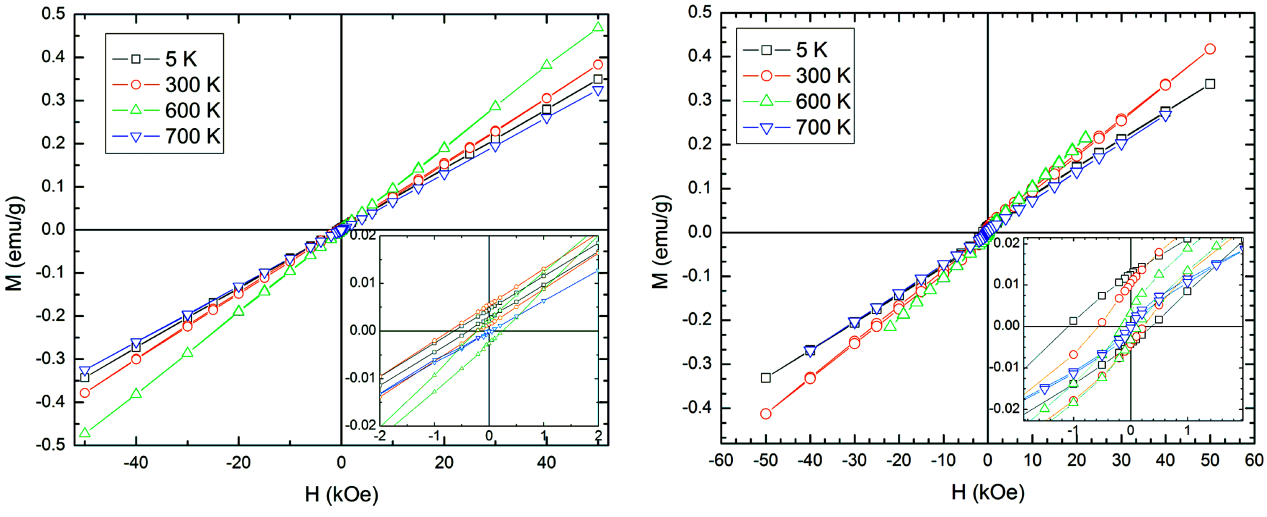

(a) (b)

Figure 4. The magnetic hysteresis loops measured at different temperatures for samples: a) CFS, b) SPS630-20 (insets show low field magnetization behaviour, 10^4 Oe = 1 T)

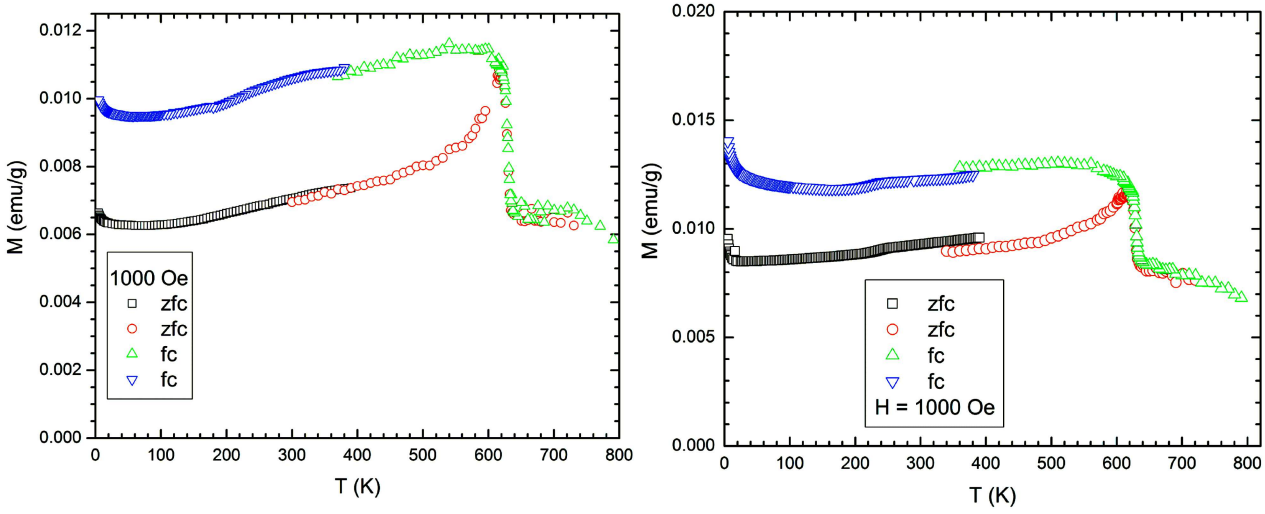

Figure 5. Temperature dependence of ZFC and FC magnetization measured in the field of 1000 Oe (0.1 T) for a) CFS sample and b) SPS650-10 sample

[30]. Our results are in good agreement with previous findings published by Dai *et al.* [30] who reported that sintering in nitrogen provided better ferroelectric properties for the samples than sintering in the air. They obtained the poorest ferroelectric properties in the samples sintered in oxygen and explained their findings by a decrease in Fe^{2+} fraction, good crystallinity and better microstructure of the samples sintered in nitrogen and air.

The magnetization (M) versus magnetic field (H) hysteresis loops at 5, 300, 600 and 700 K (Fig. 4) for the CFS and SPS630-20 samples clearly show small deviation from linear field-dependence of magnetization, which indicates antiferromagnetic order. Widening of *M-H* loops at low temperatures points to the development of weak ferromagnetism originating from the spin-spiralling [31] within antiferromagnetic order, established below the Néel temperature of about 620 K. *M-H* hysteresis loops of both samples showed a shift and coercivity enhancement at 5 K and 300 K, (insets of Fig. 4) that might be related to the exchange bias effect, as usually observed in $BiFeO_3$ [32].

The temperature dependence of magnetization for the CFS and SPS650-10 samples are shown in Fig. 5. We presented *M-T* results for sample SPS650-10 with higher amount of secondary phases (Fig. 5b) in order to clearly observe influence of $Bi_2Fe_4O_9$ phase on magnetization. Both samples showed small values of magnetization ($M \approx 0.01$ emu/g) under zero field cooling and field ($H = 1000$ Oe $= 0.1$ T) cooling (Fig. 5). Nevertheless, magnetization of the SPS sample is higher than that of the CFS samples and it is also in good agreement with results of Wang *et al.* [16], who also found enhanced magnetization in samples obtained by spark plasma sintering. The obtained magnetization values of the SPS samples are similar to values obtained by rapid liquid-phase sintering technique [33] and higher than values reported for ceramics obtained by microwave sintering [12]. Magnetization of both samples decreased as temperature decreased from 620 K to 100 K, which is typical for antiferromagnetics. In further cooling from 100 K to 4 K, the magnetization slightly increased, as shown in Fig. 5. Apparent peak in the ZFC curves and corresponding changes in the slope of FC curves at 623 K for both samples indicate the antiferromagnetic-paramagnetic transition. The small changes in the slope of ZFC curves at about 265 K correspond to the ferromagnetic-paramagnetic transition of $Bi_2Fe_4O_9$, confirming the presence of this secondary phase in both samples.

IV. Conclusions

Bismuth ferrite ceramics was obtained by conventional and spark plasma sintering of hydrothermally synthesized powders. It was found that all samples contained small amounts of secondary phases, $Bi_2Fe_4O_9$ and $Bi_{25}FeO_{39}$. The optimal processing conditions for the SPS method were 630 °C for 20 min, under uniaxial pressure of 90 MPa. The ceramics sample prepared under these conditions showed optimal relation between density and concentration of secondary phases. Although not as high as 96 %TD obtained by conventional method, spark plasma sintering also provided satisfactory densification of up to 90 %TD. On the other hand, spark plasma sintered samples showed better saturation of electric polarization and higher values of coercive field than conventionally sintered BFO.

Acknowledgement: The authors acknowledge the financial support of the Ministry of Education and Science of Republic of Serbia (project number III45007) and bilateral cooperation project between Republic of Serbia and Republic of Croatia (project title "Magnetoelectric behaviour of the transition metal oxides nanostructured multiferroic ceramics". Damir Pajić acknow-

ledges support of Croatian Science Foundation under the project UIP-2014-09-8276. Miladin Radovic acknowledges support of U.S. National Science Foundation under the grant DMR-1057155.

References

1. I. Sosnowska, R. Przenioslo, P. Fischer, V.A. Murasov, "Investigation of crystal and magnetic structure of $BiFeO_3$ using neutron diffraction", *Acta Phys. Pol. A*, **86** [4] (1994) 629–631.
2. F. Kubel, H. Schmid, "Structure of a ferroelectric and ferroelastic monodomaincrystal of the perovskite $BiFeO_3$", *Acta Crystallogr. B*, **46** (1990) 698–702.
3. C. Ederer, N.A. Spaldin, "Weak ferromagnetism and magnetoelectric couplingin bismuth ferrite", *Phys. Rev. B*, **71** [6] (2005) 060401.
4. T. Rojac, A. Bencan, B. Malic, G. Tutuncu, J.L. Jones, J.E. Daniels, D. Damjanovic, "$BiFeO_3$ ceramics: processing, electrical and electromechanical properties", *J. Am. Ceram. Soc.*, **97** [7] (2014) 1993–2011.
5. M.S. Bernardo, "Synthesis, microstructure and properties of $BiFeO_3$-based multiferroic materials: A review", *Bol. Soc. Esp. Ceram. Vidr.*, **53** (2014) 1–14.
6. J. Silva, A. Reyes, H. Esparza, H. Camacho, L. Fuentes, "$BiFeO_3$: A Review on synthesis, doping and crystal structure", *Integr. Ferroelectr.*, **126** [1] (2011) 47–59.
7. X. He, L. Gao, "Synthesis of pure phase $BiFeO_3$ powders in molten alkali metal nitrates", *Ceram. Int.*, **35** [3] (2009) 975–978.
8. I. Szafraniak, M. Polomska, B. Hilczer, A. Pietraszko, L. Kepinski, "Characterization of $BiFeO_3$ nanopowder obtained by mechanochemical synthesis", *J. Eur. Ceram. Soc.*, **27** [13-15] (2011) 4399–4402.
9. D. Maurya, H. Thota, K.S. Nalwa, A. Garg, "$BiFeO_3$ ceramics synthesized by mechanical activation assisted versus conventional solid-state-reaction process: A comparative study", *J. Alloys Compd.*, **477** [1-2] (2009) 780–784.
10. A. Perejón, N. Murafa, P.E. Sánchez-Jimenez, J.M. Criado, J. Subrt, M.J. Diánez, L.A. Pérez-Maqueda, "Direct mechanosynthesis of pure $BiFeO_3$ perovskite nanoparticles: reaction mechanism", *J. Mater. Chem. C*, **1** [22] (2013) 3551–3562.
11. Y.P. Wang, L. Zhou, M.F. Zhang, X.Y. Chen, J.M. Liu, Z.G. Liu, "Room-temperature saturated ferroelectric polarization in $BiFeO_3$ ceramics synthesized by rapid liquid phase sintering", *Appl. Phys. Lett.*, **84** [10] (2004) 1731–1733.
12. W. Cai, C. Fu, W. Hu, G. Chen, X. Deng, "Effects of microwave sintering power on microstructure, dielectric, ferroelectric and magnetic properties of bismuth ferrite ceramics", *J. Alloy Compd.*, **554** (2013) 64–71.
13. S.H. Song, Q.S. Zhu, L.Q. Weng, V.R. Mudinepalli, "A comparative study of dielectric, ferroelectric and magnetic properties of $BiFeO_3$ multiferroicceramics synthesized by conventional and spark plasma sintering techniques", *J. Eur. Ceram. Soc.*, **35** [1] (2015) 131–138.
14. A. Perejón, N. Masó, A.R. West, P.E. Sánchez-Jiménez, R. Poyato, J.M. Criado, L.A. Pérez-Maqueda, "Electrical properties of stoichiometric $BiFeO_3$ prepared by mechanosynthesis with either conventional or spark plasma sintering", *J. Am. Ceram. Soc.*, **96** [4] (2013) 1220–1227.
15. A. Perejón, P.E. Sánchez-Jiménez, R. Poyato, N. Masó, A.R. West, J.M. Criado, L.A. Pérez-Maqueda, "Preparation of phase pure, dense fine grained ceramics by conventional and spark plasma sintering of La-substituted $BiFeO_3$ nanoparticles", *J. Eur. Ceram. Soc.*, **35** [8] (2015) 2283–2293.
16. L.C. Wang, Z.-H. Wang, S.L. He, X. Li, P.T. Lin, J.R. Sun, B.G. Shen, "Enhanced magnetization and suppressed current leakage in $BiFeO_3$ ceramics prepared by spark plasma sintering of sol-gel derived nanoparticles", *Physica B*, **407** [8] (2012) 1196–1202.
17. D. Luković Golić, A. Radojković, J. Ćirković, A. Dapčević, D. Pajić, N. Tasić, S.M. Savić, M. Počuča-Nešić, S. Marković, G. Branković, Z. Marinković Stanojević, Z. Branković, "Structural, ferroelectric and magnetic properties of $BiFeO_3$ synthesized by sonochemically assisted hydrothermal and hydro-evaporation chemical methods", *J. Eur. Ceram. Soc.*, **36** [7] (2016) 1623–1631.
18. Z.-H. Dai, Y. Akishige, "$BiFeO_3$ ceramics synthesized by spark plasma sintering", *Ceram. Int.*, **38** (2012) S403–S406.
19. Z. Dai, Y. Akishige, "Electrical properties of multiferroic $BiFeO_3$ ceramics synthesized by spark plasma sintering", *J. Phys. D: Appl. Phys.*, **43** (2010) 445403.
20. R.G. Garvey, "Computer comments", *Powder Diffr.*, **1** (1986) 114–118.
21. J. Rodriguez-Carvajal, F*ULLPROF: A program for Rietveld refinement and pattern matching analysis*, Version 1.9c. France, 2001.
22. L. Hu, R. Benitez, S. Basu, I. Karaman, M. Radovic, "Processing and characterization of porous Ti_2AlC with controlled porosity and pore size", *Acta Mater.*, **60** [18] (2012) 6266–6277.
23. T. Wang, S.-H. Song, M. Wang, J.-Q. Li, M. Ravi, "Effect of annealing atmosphere on the structural and electrical properties of $BiFeO_3$ multiferroic ceramics prepared by sol-gel and spark plasma sintering techniques", *Ceram. Int.*, **42** [6] (2016) 7328–7335.
24. O. Guillon, J. Gonzalez-Julian, B. Dargatz, T. Kessel, G. Schierning, J. Rathel, M. Herrmann, "Field-assisted sintering technology/spark plasma sintering: Mechanisms, materials, and technology developments", *Adv. Eng. Mater.*, **16** [7] (2014) 830–849.
25. A. Reyes, C. Vega, M. E. Fuentes, L. Fuentes,

"$BiFeO_3$: Synchrotron radiation structure refinement and magnetoelectric geometry", *J. Eur. Ceram. Soc.*, **27** [13-15] (2007) 3709–3711.
26. X.Z. Chen, Z.C Qiu, J.P. Zhou, G. Zhu, X.B Bian, P. Liu, "Large-scale growth and shape evolution of bismuth ferrite particles with a hydrothermal method", *Mater. Chem. Phys.*, **126** [3] (2011) 560–567.
27. M. Yasin Shami, M.S. Awan, M. Anis-ur-Rehman, "Phase pure synthesis of $BiFeO_3$ nanopowders using diverse precursor via co-precipitation method", *J. Alloy Compd.*, **509** [41] (2011) 10139–10144.
28. P. Uniyal, K.L. Yadav, "Room temperature multiferroic properties of Eu doped $BiFeO_3$", *J. Appl. Phys.*, **105** [7] (2009) 07D914.
29. K.B. Chong, F. Guiu, M.J. Reece, "Thermal activation of ferroelectric switching", *J. Appl. Phys.*, **103** [1] (2008) 014101.
30. H.Y. Dai, Z.P. Chen, T. Li, R.Z. Xue, J. Chen, "Structural and electrical properties of bismuth ferrite ceramics sintered in different atmospheres", *J. Supercond. Nov. Magn.*, **26** (2013) 3125–3132.
31. M. Mostovoy, "Ferroelectricity in spiral magnets", *Phys. Rev. Lett.*, **96** [6] (2006) 067601.
32. Z.-Z. Ma, Q. Jian, Z.-P. Chen, Z.-M. Tian, X.-J. Hu, H.-J. Huang, "Multiferroic properties and exchange bias in $Bi_{1-x}Sr_xFeO_3$ (x = 0–0.6) ceramics", *Chin. Phys. B*, **23** [9] (2014) 097505–097510.
33. A.K. Pradhan, K. Zhang, D. Hunter, J.B. Dadson, G.B. Loutts, P. Bhattacharya, R. Katiyar, J. Zhang, D.J. Sellmyer, U.N. Roy, Y. Cui, A. Burger, "Magnetic and electrical properties of single-phase multiferroic $BiFeO_3$", *J. Appl. Phys.*, **97** (2005) 093903.